

The Effect of Irregular Seismic Loading and Soil Density on the Liquefaction Behavior of Saturated Sand

Bahareh Katebi¹, Abbas Ghalandarzadeh^{2*}, Mehdi Derakhshandi¹, Navid Ganjian¹

¹ Department of Civil Engineering, Science and Research Branch, Islamic Azad University, postal code Tehran, Iran

² School of Civil Engineering, College of Engineering, University of Tehran, postal code Tehran, Iran

* Corresponding author, e-mail: aghaland@ut.ac.ir

Received: 11 January 2022, Accepted: 11 June 2023, Published online: 11 July 2023

Abstract

Structures located on sandy soils can be significantly damaged by earthquake-induced liquefaction. A series of stress-controlled cyclic triaxial tests under harmonic and irregular loading under various soil densities 30%, and 50%, was conducted to evaluate the effects of irregularities and relative densities on the liquefaction characteristics of saturated sand. The irregular actual ground motions time histories obtained from six stations of the 1999 Chi-Chi Earthquake and harmonic sinusoidal cyclic loading time histories were applied to Firoozkooh #161 sand specimens, and the results were compared in terms of the type waveforms loading and relative densities. Based on the stress and energy method, the Correction coefficient is calculated for a variety of densities and types of irregular loading. The present results reveal that it is not precise to assume a single correction coefficient for all records, regardless of the complicated time-domain characteristics of ground motions. Furthermore, the results indicate that the relative soil density and the type of irregular loading influenced sand's pore pressure generation and liquefaction potential.

Keywords

liquefaction, triaxial tests, Firoozkooh sand, irregular loading

1 Introduction

Liquefaction is a soil mechanics problem that often influences structures supported on saturated sand deposits. Sladen et al. [1] State that liquefaction occurs when a mass of soil loses a large percentage of its shear resistance when subjected to monotonic, cyclic, or shock loading. Seismic waves, traffic, and wind are sources of harmonic sinusoidal cyclic loading that may cause the liquefaction failure of sand. These loads are applied randomly and may include a sequence of erratic cyclic amplitudes of stress pulses [2–7]. The averaging method is usually used for cyclic testing in the laboratory [2, 8–12].

Seed and Idriss [13] proposed an equivalent approach, and Seed et al. [14] evaluated the equivalent uniform cyclic stress as 65% of the maximum stress in random loadings. Even though major refinements have been made to evaluate soil liquefaction resistance, the Cyclic Stress Ratio (CSR), a dimensionless quantity used to quantify the magnitude of cyclic loading in materials and the most typical way to characterize an earthquake loading, is still mainly based on the framework developed by Seed and Idriss [13]. But this approach cannot capture all aspects of the complicated time-domain characteristics of ground motions [15].

Ishihara and Yasuda [16] conducted a series of liquefaction tests using random time histories. They proposed that the correction factor (the ratio of the uniform stress amplitude to the maximum shear stress in random loading trace) should be between 0.41 and 0.72, depending upon the amplitude of the stress pulses.

Recent research has evaluated sand behavior under random loading [17]. Du and Chian [18] conducted cyclic strain triaxial testing to investigate soil liquefaction of clean sand under non-uniform loading. In uniform strain-controlled cyclic tests, they showed that large strain amplitudes produce a more rapid generation of excess pore pressure. In non-uniform strain-controlled tests, larger strain amplitudes may generate lower excess pressure.

Pan and Yang [19] carried out a systematic experimental investigation into the liquefaction potential of sand subjected to harmonic sinusoidal cyclic loading under random time histories. The results indicated that pore pressure generation and the liquefaction resistance of sand are significantly influenced by the amplitude and sequence of the stress pulses in random loadings. Instances of investigation of soil response in the laboratory using real

earthquake motion are very limited [16, 20–23]. An alternative method that utilizes the dissipated energy concept was introduced by Nemat-Nasser and Shokooh [24].

In recent decades, some experimental research has explored the effects of some factors such as the effective confining pressure, relative density of sand, and consolidation stress ratio, on the relationship between incremental pore water pressure and dissipated energy [25–30]. The effect of the fine content and particle size distribution of sand on the energy versus pore pressure relationship was also investigated [31–33].

Jafarian et al. [34] and Pan and Yang [35] argued that the required dissipated energy increases with the applied static shear stress. It can be concluded from the literature that the energy approach is a simple but practical method for the evaluation of liquefaction potential. However, most studies have been performed on specimens subjected to uniform cyclic loads. This is due to the lack of facilities to apply irregular loads to specimens. Furthermore, the effects of harmonic sinusoidal cyclic loading on specimens of various densities have not been considered.

In the current study, the effects of irregular loading of strong ground motions, including two patterns of shock and vibration ground motion, are applied to the sand samples, and the liquefaction potential and pore water pressure characteristics of Firoozkooch #161 (also known as Firuzkuh and Firozkooh) in various densities are compared with those results which are obtained from the same specimens subjected to harmonic sinusoidal cyclic loading. Moreover, correction coefficients are introduced and used to approximate the irregular earthquake loading to harmonic sinusoidal cyclic loading. Coefficients can be used for evaluating liquefaction potential for facilities that cannot apply irregular loading to specimens of sand in a variety of relative soil densities.

2 Methods: experiment program

2.1 Soil properties

The physical specifications of the Firoozkooch #161 sand such as specific gravity (G_s), minimum and maximum void ratio (e_{min} , e_{max}), uniformity coefficient (C_u), curvature coefficient (C_c) used in this research are presented in Table 1 and Fig. 1. As shown in Fig. 1, the Firoozkooch sand falls within the grain-size distribution range of liquefiable soils [36].

Table 1 The physical specifications of Firoozkooch sand

sand	G_s	e_{min}	e_{max}	C_u	C_c
Firoozkooch 161	2.65	0.555	0.916	2.28	0.952

2.2 Test procedure

Cyclic triaxial test specimens 50 mm in diameter and 100 mm in height were prepared in watertight rubber membranes with porous stone and filter paper on each end (Fig. 2). The wet tamping method was used for sampling. Five layers of 350 g were compacted using a hand tamper until the desired density was reached. This method enables preparing reconstituted soil samples at a wide range of initial densities with a high degree of precision and provides more isotropic fabric samples [37–39].

Carbon dioxide and de-aired water were circulated through the specimen to achieve a high degree of saturation. To ensure the full saturation of the soil, Skempton's pore pressure parameter B ($\Delta u/\Delta\sigma_3$) was calculated. For each specimen, we measured the increase in pore water pressure Δu , induced by increasing cell pressure by $\Delta\sigma_3$. Fully saturation was defined when B greater than 0.96 was achieved. The saturated specimen was isotropically consolidated to a confining pressure of 100 kPa. After consolidation, soil specimens were subjected to cyclic uniform or irregular time histories under undrained conditions (stress-controlled) until initial liquefaction had occurred [40, 41].

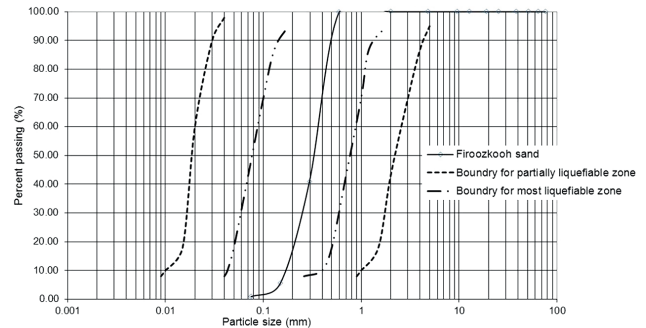


Fig. 1 Grain size distribution of Firoozkooch sand

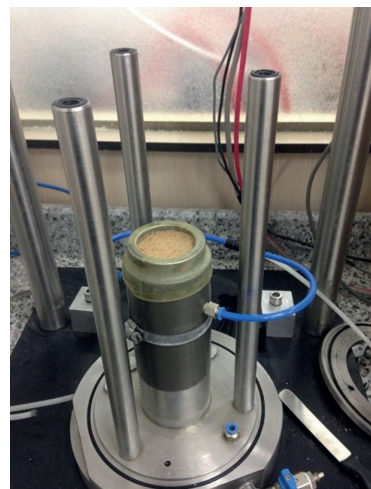


Fig. 2 Vacuum mold

The experiments performed in this research used relative densities (Dr) of 30% and 50%. The ($Dr = (e_{max} - e) / (e_{max} - e_{min})$) index is another measure of void ratio based on global void ratios. This is a general index of soil density that determines the void ratio between the upper and lower limits of the soil [41]. All tests were performed at a similar relative density, and all samples were prepared using the method described above.

2.2.1 Generation of random loading

To generate an earthquake type of loading, different earthquake time histories were used. Since there is a proportional relation between the shear stress acting on a soil element at a certain depth and the ground acceleration [13, 16, 20], this pattern of acceleration time history was used to obtain loading time histories for driving the triaxial device.

To evaluate the irregular shear stress (τ) history induced by a real-time earthquake at any depth z within a soil deposit, the approach proposed by Seed and Idriss [13], as exhibited by Eq. (1), has been adopted.

$$\tau = (acc.(g) / g) \times \sigma'_c \times r_d,$$

$$r_d = 1.0 - 0.00765 \times z \rightarrow z \leq 9.15 \text{ m}, \tag{1}$$

$$r_d = 1.174 - 0.0267 \times z \rightarrow 9.15 \leq z \leq 23 \text{ m},$$

where $acc.(g)$ is the acceleration time history, σ'_c is the effective confining stress, and r_d is the stress reduction factor (Eq. (2); [42]) accounting for the deformable characteristics of the soil specimen. The deviatoric stress history was derived from the strong motion stress history. The cyclic stress ratio (CSR) of harmonic sinusoidal cyclic loading can be evaluated as $q_{max} / 2 \sigma'_c$ that q is the maximum shear stress that liquefaction happened.

In this research, the time histories were categorized based on the following criteria: if the wave had only one or two peaks with amplitudes greater than 60% of the maximum acceleration, it was classified as a shock-type wave. Alternatively, if the waveform on the side of the maximum acceleration contained more than three peaks with amplitudes greater than 60% of the maximum, the wave was classified as a vibration-type wave [20]. Table 2 provides the classification of each waveform.

2.3 Test program

In the present study, the records of the 1999 Chi-Chi Earthquake in Taiwan were analyzed. The waveforms were categorized based on their shape, as vibrations and shocks. Thus, to investigate the effect of irregularity on loading,

three shock patterns and three vibration deviator stress patterns were used. The specifications of these records are shown in Table 2. Several specimens were tested under harmonic sinusoidal cyclic loading to study the effect of irregular loading on the liquefaction potential of sand.

2.3.1 Uniform cyclic test results

In this research, the data collected from the series of uniform cyclic stress-controlled triaxial tests were used to investigate the effect of the irregularity of loading. The relative densities of the specimens were 30% and 50%, and the consolidation stress was $\sigma'_c = 100$ kPa. Table 3 summarizes the conditions for all cyclic tests performed in this study. The applied uniform CSR versus the number of cycles required to cause liquefaction is plotted in Fig. 3.

Table 2 The specification of the records of the 1999 Chi-Chi Earthquake

NO	Station Name	Type of loading	a_{max} (g)
1	"CHY057"	vibration	0.05
2	"CHY061"	vibration	0.04
3	"CHY062"	vibration	0.06
4	"CHY025"	shock	0.17
5	"TCU026"	shock	0.12
6	"TCU076"	shock	0.42

Table 3 The conditions of all cyclic tests

Test number	Test parameters		
	Effective confining stress σ'_c (kPa)	Dr (%)	Cyclic stress ratio (CSR)
1	100	30	0.15
2	100	30	0.23
3	100	30	0.25
4	100	50	0.2
5	100	50	0.25
6	100	50	0.3

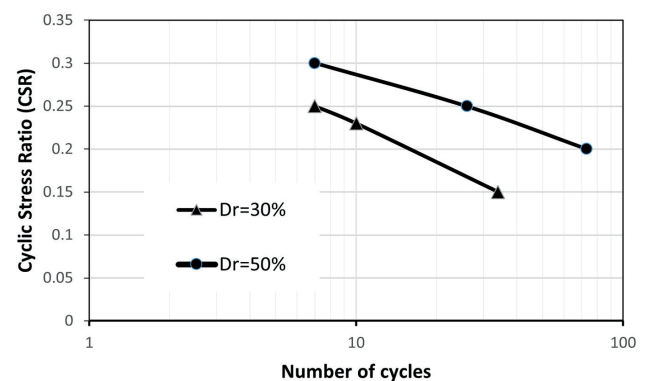


Fig. 3 Uniform Cyclic stress ratio CSR versus the number of cycles required to cause liquefaction

As shown in Fig. 3, the specimen was liquefied at higher cycles of uniform loading while the applied CSR decreased. This figure shows the CSR of soil liquefaction at relative densities of 30% and 50%, and consolidation stress for any number of cycles can be calculated accurately. Furthermore, it shows the effect of the relative density of specimens on the liquefaction potential wherein denser Firoozkooch sand ($D_r = 50\%$) has higher liquefaction resistances than the looser one ($D_r = 30\%$) at different stress levels. These results are in agreement with those of several previous studies. [43–45].

It can be deduced from Fig. 3, that similar to previous studies, sand under increased uniform harmonic sinusoidal cyclic loading and smaller relative density values have the greatest potential for liquefaction.

2.3.2 Irregular loading test results

In the first step, the loading intensity (for example, Fig. 4) did not result in the liquefaction of the specimen. As shown in Fig. 4, the pore-water pressure (r_u) increased gradually before maximum stress occurred but increased abruptly as it approached maximum stress and then remained constant. The maximum deviator stress and the ratio of residual pore-water pressure relevant to the loading patterns are described below. In the next step, the intensity of the applied loading increased slightly as the waveform remained

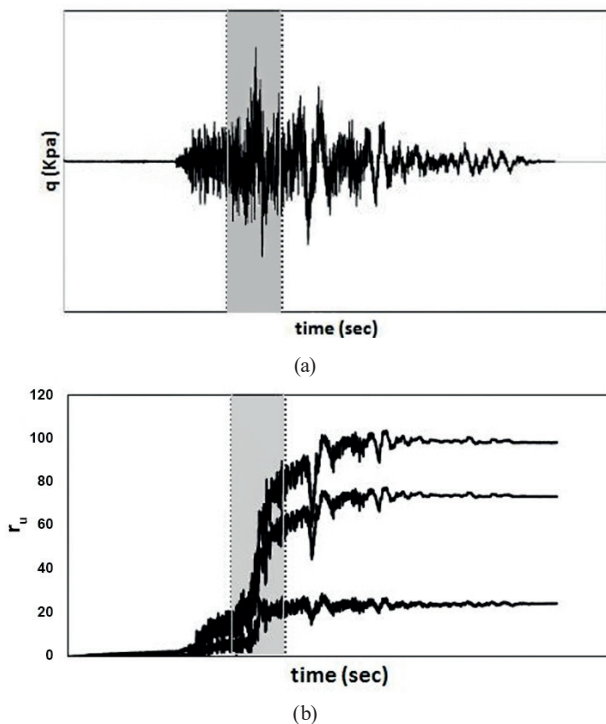


Fig. 4 Example of increase in r_u during irregular loading (a) stress versus time, (b) excess pore water pressure versus time

constant. The steps were repeated until the increase in pore-water pressure was equal to the initial effective multi-lateral stress that caused liquefaction. Table 4 summarizes the conditions of all irregular tests performed in this study. The change in the residual pore-water pressure ratio (r_u) during loading is shown in Figs. 5 to 7.

Table 4 The conditions of all irregular tests

Test ID	Test parameters			
	Type of loading	D_r (%)	Max. stress ratio	Effective onfining stress σ'_c (kPa)
1-30-1	vibration	30	0.19	100
1-30-2	vibration	30	0.25	100
1-30-3	vibration	30	0.28	100
2-30-1	vibration	30	0.19	100
2-30-2	vibration	30	0.23	100
2-30-3	vibration	30	0.28	100
3-30-1	vibration	30	0.19	100
3-30-2	vibration	30	0.3	100
3-30-3	vibration	30	0.38	100
4-30-1	shock	30	0.19	100
4-30-2	shock	30	0.35	100
4-30-3	shock	30	0.43	100
5-30-1	shock	30	0.19	100
5-30-2	shock	30	0.45	100
5-30-3	shock	30	0.52	100
6-30-1	shock	30	0.19	100
6-30-2	shock	30	0.35	100
6-30-3	shock	30	0.47	100
1-50-1	vibration	50	0.26	100
1-50-2	vibration	50	0.3	100
1-50-3	vibration	50	0.34	100
2-50-1	vibration	50	0.26	100
2-50-2	vibration	50	0.3	100
2-50-3	vibration	50	0.34	100
3-50-1	vibration	50	0.26	100
3-50-2	vibration	50	0.35	100
3-50-3	vibration	50	0.43	100
4-50-1	shock	50	0.26	100
4-50-2	shock	50	0.45	100
4-50-3	shock	50	0.5	100
5-50-1	shock	50	0.26	100
5-50-2	shock	50	0.45	100
5-50-3	shock	50	0.57	100
6-50-1	shock	50	0.26	100
6-50-2	shock	50	0.45	100
6-50-3	shock	50	0.52	100

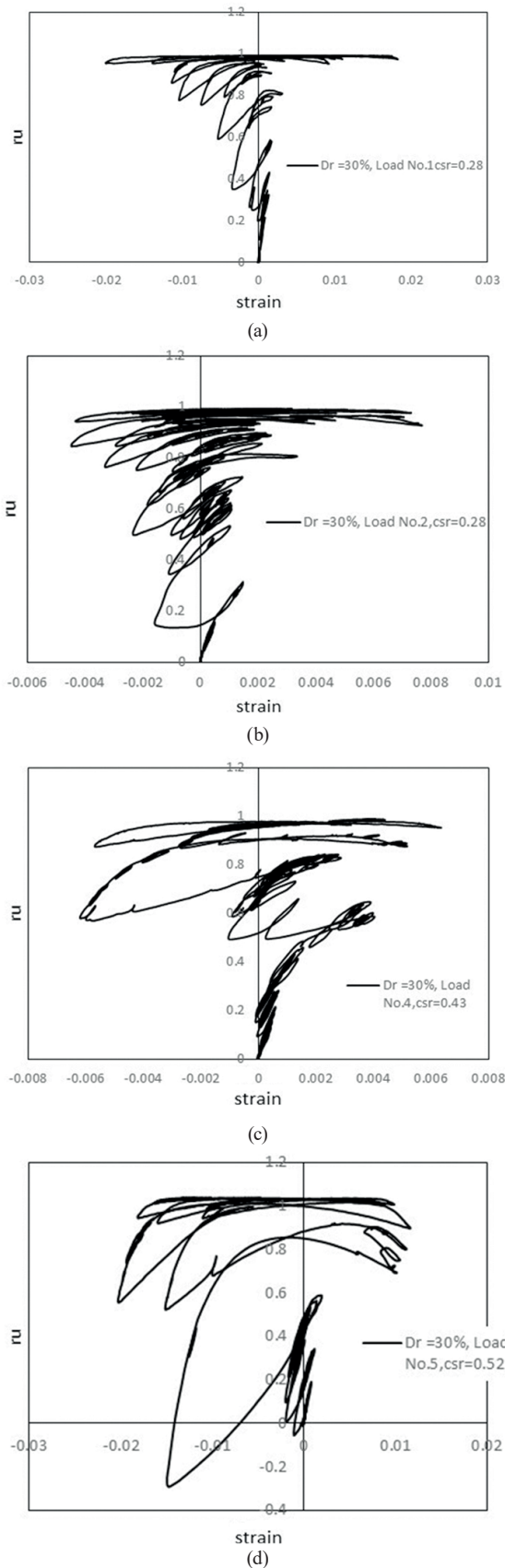


Fig. 5 Excess pore water pressure ratio versus strain for irregular loading at $Dr = 30\%$ (a) load No.1, $CSR = 0.28$, (b) load No.2, $CSR = 0.28$, (c) load No.4, $CSR = 0.43$, (d) load No.5, $CSR = 0.52$

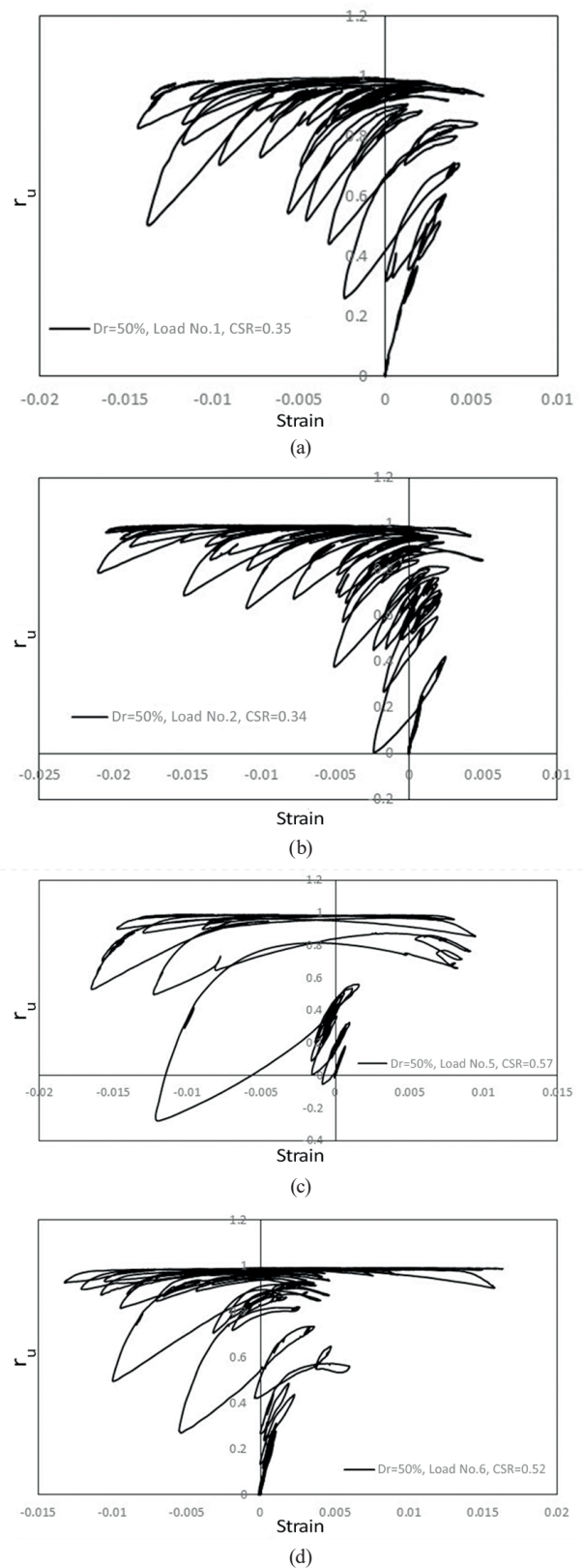


Fig. 6 Excess pore water pressure ratio versus strain for irregular loading at $Dr = 50\%$ (a) load No.1, $CSR = 0.34$, (b) load No.2, $CSR = 0.34$, (c) load No.5, $CSR = 0.57$, (d) load No.6, $CSR = 0.52$

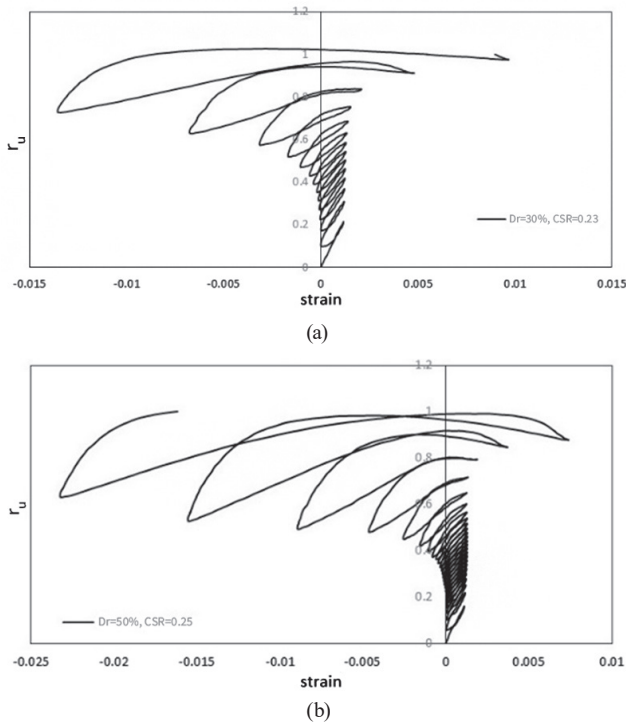


Fig. 7 Excess pore water pressure ratio versus strain for harmonic sinusoidal cyclic loading (a) $D_r = 30\%$, $CSR = 0.23$, (b) $D_r = 50\%$, $CSR = 0.25$

The specimens had a consolidation stress of $\sigma'_c = 100$ kPa and a relative density of $D_r = 30\%$ and 50% . Because of the complicated form of time histories, the biggest change in pore pressure occurred when the maximum deviator stress was applied to the specimen. The maximum deviator stress is defined as $CSR_{max} = q_{max}/2\sigma'_c$.

The results from shock records indicate that the abrupt increase in pore-water pressure occurred when acceleration reached its maximum value, and that maximum acceleration was applied suddenly to the specimen. For vibrational records, the maximum vibrational acceleration was used more uniformly so the pore-water pressure increased gradually over time.

3 Discussion

The 6 records of the 1999 Chi-Chi Earthquake were examined from different stations. As mentioned before, the records at stations 4, 5, and 6 were shock loading, and records at stations 1, 2, and 3 were vibration waveforms. Stress-controlled cyclic triaxial tests at different soil relative densities (30%, 50%) under undrained conditions were conducted on specimens as summarized in Table 4.

As a means of studying soil behavior under shock and vibration waveforms more precisely, the variation of excess pore pressure at different Peak Ground Accelerations (PGA), which subject the soil to liquefaction,

was investigated at relative densities of 30 and 50 percent. The results show that, by increasing the relative density of specimens, the PGA of record that leads to liquefaction increased. Thus, relative density has a major role in defining the dynamic behavior of cohesionless soils [2, 46].

The number of acceleration cycles that reached 0.65 PGA in each record was examined to evaluate soil behavior under shock and vibration loading more accurately. Therefore, the number of cycles for vibrational records was higher than for shock records, so samples under this type of loading required less PGA to liquefy the soil.

To compare the trend of increasing excess pore water pressure during loading over time and to examine the behavior of soil settlement at different relative densities, Figs. 5 to 7 were plotted.

According to Fig. 5 and 6, for shock loading, the increase of strain versus excess pore water pressure for all the considered soil relative densities occurred suddenly at a few strain pulses, while the stiffness of soil decreased rapidly upon the triggering of liquefaction ($r_u = 1.0$).

Figs. 5 to 7 demonstrate that since the number of cycles in the vibrational records was much higher than shock loading, the specimen's behavior under harmonic sinusoidal cyclic loading was similar to vibration loading.

3.1 Correction coefficient and the equivalent number of cycles in random loading, based on the stress method

The ratio of uniform shear stress which liquefies the soil during N cycles is denoted as $(q_{u,l}/2\sigma'_c)N$. The effect of irregularity and complex shape of waves on the soil is called the correction coefficient and obtained as:

$$C_{irr} = \frac{(q_{u,l}/2\sigma'_c)N}{(q_{max,l}/2\sigma'_c)}, \quad (2)$$

in which N is the number of equivalent cycles and the value of $(q_{u,l}/2\sigma'_c)N$ and $(q_{max,l}/2\sigma'_c)$ are obtained from the results of uniform and irregular loadings, respectively. Table 5 summarizes the correction coefficient values obtained from all the tests conducted in the current study. The Cyclic Stress Ratio (CSR), denoted as $(q_{u,l}/2\sigma'_c)_{20}$, represents the level of cyclic loading applied over 20 cycles that causes soil liquefaction. This number represents an earthquake of magnitude 7.5 [10].

Based on Table 5, it can be concluded that the C_{irr} for shock loading was lower than for vibration loading. Therefore, the cyclic strength of the soil against shock loads was greater than vibration loads, and as the C_{irr} approached the value of 1.0, waveforms with irregular loading became more uniform.

According to previous studies on the type of stress, such as Seed et al. [14], the equivalent shear stress was selected to be 65% of the maximum shear stress of random loading.

Ishihara and Yasuda conducted several liquefaction experiments with irregular loading for cyclic triaxial and torsional shear tests. They concluded that the shear stress was equivalent to 57% of the maximum shear stress and 20 cycles had almost the same effect [16, 20].

Table 5 presents that C_{irr} for the shock type of loading at relative densities of 30% and 50% were 0.38 and 0.48 and for the vibration type were 0.59 and 0.69, respectively. Additionally, as the relative density of the specimens

increased (30% to 50%), the correction factor of the sand increased as well. It is noteworthy that relative density plays a significant role in governing the onset of liquefaction of cohesionless specimens subjected to seismic loading.

3.2 Correction coefficients based on the number of cycles that reached 0.65PGA

As shown in Table 6, the correction coefficients are listed according to the number of acceleration cycles that reached 0.65PGA (N) at all considered values of the relative density of the soil for each record. The values of (N) for vibrations (indicated in Table 2) were 13, 9, and 6, while the value for shock loading was 3.

Table 5 Correction coefficients for relative densities of 30% and 50%, based on equivalent 20 cycles

No		$\frac{q_{max,l}}{2\sigma'_c}$	$\left(\frac{q_{max,l}}{2\sigma'_c}\right)_{av}$	$\left(\frac{q_{u,l}}{2\sigma'_c}\right)_{20}$	C_{irr}	$(C_{irr})_{av}$
1		0.35			0.743	
2	Vibration type	0.36	0.39	0.26	0.722	0.69
3		0.43			0.6	
4		0.5			0.52	
5	Shock type	0.6	0.55	0.26	0.433	0.48
6		0.55			0.473	
<hr/>						
1		0.3			0.633	
2	Vibration type	0.29	0.34	0.19	0.655	0.59
3		0.43			0.48	
4		0.45			0.42	
5	Shock type	0.55	0.5	0.19	0.34	0.38
6		0.5			0.38	

Table 6 Correction coefficients for relative densities of 30% and 50%, based on the number of cycles that reached 0.65 PGA

No		$\frac{q_{max,l}}{2\sigma'_c}$	$\left(\frac{q_{max,l}}{2\sigma'_c}\right)_{av}$	$\left(\frac{q_{u,l}}{2\sigma'_c}\right)_N$	C_{irr}	$(C_{irr})_{av}$
1		0.35		0.28	0.81	
2	Vibration type	0.36	0.39	0.29	0.8	0.76
3		0.43		0.29	0.68	
4		0.5		0.3	0.59	
5	Shock type	0.6	0.55	0.3	0.49	0.54
6		0.55		0.3	0.54	
<hr/>						
1		0.3		0.22	0.73	
2	Vibration type	0.29	0.34	0.24	0.83	0.73
3		0.4		0.25	0.63	
4		0.45		0.26	0.58	
5	Shock type	0.55	0.5	0.26	0.47	0.52
6		0.5		0.26	0.52	

Table 6 presents that the C_{irr} for the shock type of loading at relative densities of 30% and 50% were 0.52 and 0.54, and for the vibration type were 0.73 and 0.76, respectively. Furthermore, the sand correction factor increased as the relative density of the specimens increased. The results indicate that density has a direct impact on the liquefaction equivalent CSR values.

Comparing the C_{irr} calculated from Tables 5 and 6, the values in Table 6 were about 20% higher than those in Table 5, which were based on previous studies that assumed liquefaction occurs after about 20 sinusoidal harmonic cycles [16, 20]. The stress correction coefficient for the shock loading waveform was lower than for the vibration waveform across all considered relative densities. Since more acceleration cycles reached 0.65PGA in the vibration waveform than in the shock waveform, the stress correction coefficient for the shock loading waveform was lower than the vibration waveform in all considered relative densities.

Therefore, it is not precise to assume a single correction coefficient for all records, regardless of the characteristics of ground motions.

3.3 Correction coefficient and the equivalent number of cycles in random loading, based on the energy method

Firstly, in order to use the energy method, it is necessary to calculate the dissipated energy inside the specimens during loading, during liquefaction, and even after that. The dissipated energy per unit volume is the surrounding area inside the hysteresis loops which is calculated in a cumulative form. Thus, to determine the dissipated energy per unit volume, the hysteresis loops of each experiment should be plotted first. According to Eq. (3), the energy per unit volume and the hysteresis curves are computed (ΔW):

$$\Delta W = \frac{1}{2} \sum_{i=1}^{n-1} (\sigma_{d,i+1} + \sigma_{d,i}) (\epsilon_{d,i+1} - \epsilon_{d,i}), \quad (3)$$

where $\sigma_{d,i}$ is the i^{th} increment in deviatoric stress, $\epsilon_{d,i}$ is the i^{th} increment in axial strain, and n is the total number of increments.

In general, the GMP (Green, Mitchell, and Polito) approach is commonly used in technical literature when examining energy criteria. In this model, residual excess pore pressure r_u , is accurately related to the amount of energy dissipated per unit volume of soil through a simple and accurate relationship:

$$r_u = \sqrt{\frac{\Delta W}{PEC}}, \quad (4)$$

where r_u and ΔW were defined previously, and pseudo energy capacity (PEC) is a calibration parameter [47].

PEC is used only as a measure of liquefaction energy in these studies. The GMP model is not used to determine the relationship between r_u and ΔW since the incremental trend of r_u in this study is similar to that of this model but does not possess thorough numerical consistency.

To determine a relation between r_u and ΔW for the tests in this research, some changes should be applied to the relation of the GMP model.

PEC can be determined from experimental data by plotting r_u versus ΔW . The PEC is the value on the horizontal axis corresponding to the intersection of a straight line drawn through the origin and the point of $r_u = 0.65$ and a horizontal line drawn at $r_u = 1.0$. This process of determining PEC is illustrated graphically in Fig. 8.

This method in geometric form is shown in the following figures for the determination of PEC in all experiments. In other words, it can be stated that PEC is approximately the same as ΔW at the start of liquefaction.

There are two reasons to use PEC instead of ΔW . Firstly, a common ΔW , which leads to liquefaction cannot be obtained for all tests by the same method. However, the PEC determination method provides this standard procedure for all tests, including those with random loading. Secondly, when the ratio of the residual pore-water pressure (r_u) under the effect of harmonic sinusoidal cyclic loading reaches $r_u = 0.65$, the specimen reaches the liquefaction stage and loses its strength, and large strains are observed in it. In the following, the figures of the r_u versus ΔW , are plotted for random and harmonic sinusoidal cyclic loading.

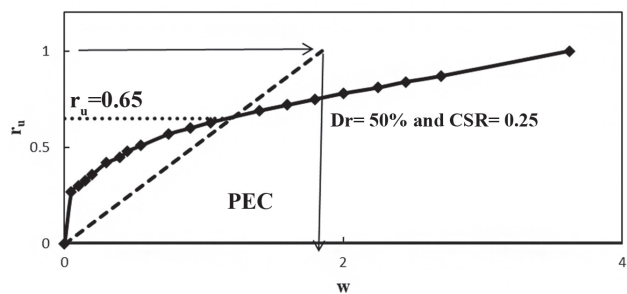


Fig. 8 Graphic illustration of how PEC is determined from experimental data. The data shown in this figure is from a cyclic triaxial test conducted on the specimen under $CSR = 0.25$

To determine the amount of PEC, Fig. 9 should be plotted. It shows that the ΔW and r_u results of the experiments with random loading had a form dependent on the form of random loading. However, when considering a constant form of random loading with different stress ratios, the forms of ΔW and r_u were found to be similar to the various PECs, indicating consistency in their behavior. By plotting Fig. 9, the amount of PEC was calculated.

3.3.1 Changes of the PEC respecting the applied CSR in harmonic sinusoidal cyclic loading and random loading

Once the plots and PECs were obtained for all experiments involving cyclic and random loading, the results were compiled and presented in Fig. 10 to facilitate a more effective comparison among them.

Fig. 10 shows the comparison of PEC for specimens under similar relative densities and different types of loadings. It can be seen that by increasing the CSR of specimens under harmonic sinusoidal cyclic loading, the PEC has been decreased. The reason for the increase of the PEC in the case of CSR reduction is that when CSR, i.e., the applied deviator stress in each cycle, is low, the specimen liquefies at a higher number of cycles (Fig. 3). This means that the specimen experiences more changes in the sign of deviator stress.

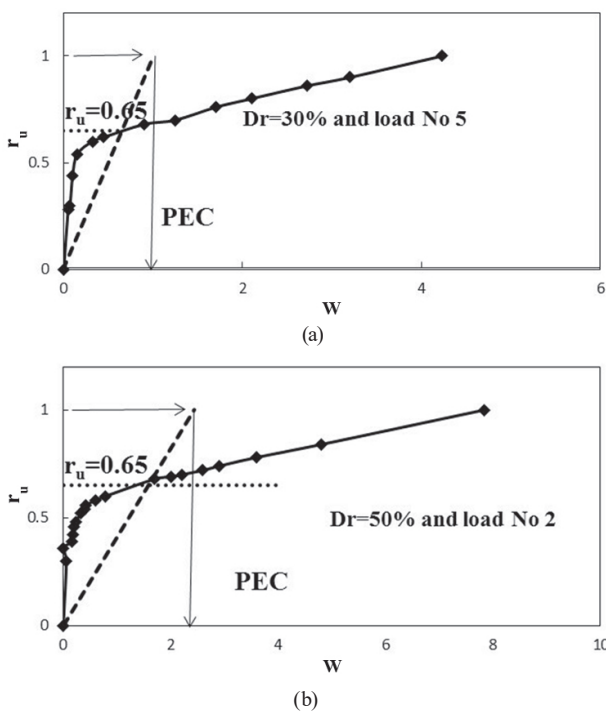


Fig. 9 Determined PEC for random loading (a) Load No.5, shocked loading, $D_r = 30\%$, (b) Load No.2, vibrational loading, $D_r = 50\%$

As shown in Fig. 10, in the shock waveforms (load No.4, 5, and 6), the PEC is less than the vibration patterns (load No. 1, 2, and 3), especially at the relative density of 50 percent.

The correction coefficients and equivalent cycle count in random loading can be determined via the energy approach. This requires plotting the obtained results on a single figure, as depicted in Fig. 11. With this information, the harmonic sinusoidal equivalent CSR was derived from the average of the PEC of both shock and vibration random loading patterns.

To clarify the procedure, arrows have been added to the figure to illustrate the steps to calculate the equivalent CSR for the average values of random loading.

The correction coefficient based on the energy method was obtained from Eq. (2) and summarized in Table 7.

The PECs for shock waveforms and vibrational waveforms at various densities are shown in Table 7. It shows that with an increase in the relative density of the specimens (30 and 50%), the correction factor of the sand increased. The results indicate that density has a direct impact on the liquefaction equivalent CSR values.

According to Tables 5–7, the stress correction coefficient for the shock loading waveform was lower than the vibration waveform at all considered values of the relative density of the soil. Therefore, it is not precise to assume a single correction coefficient for all records, regardless of the

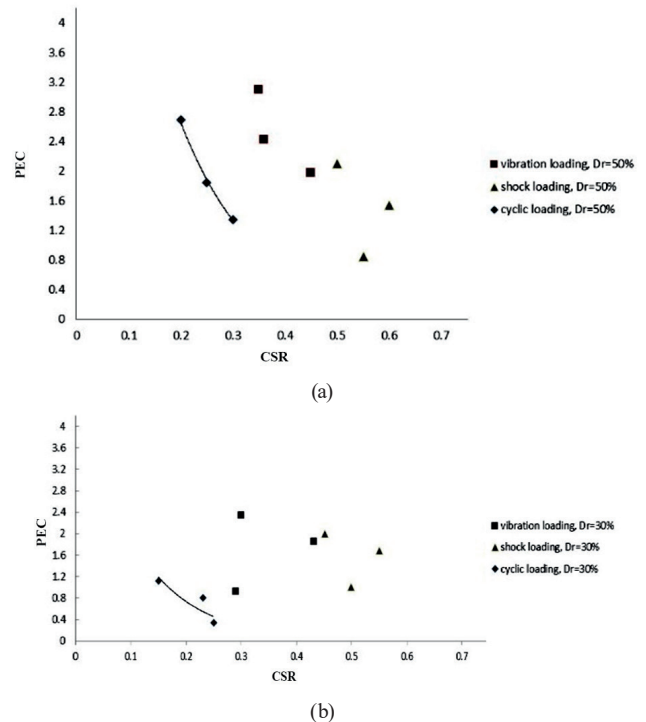


Fig. 10 PEC versus CSR for all the considered types of loading (a) $D_r = 30\%$, (b) $D_r = 50\%$

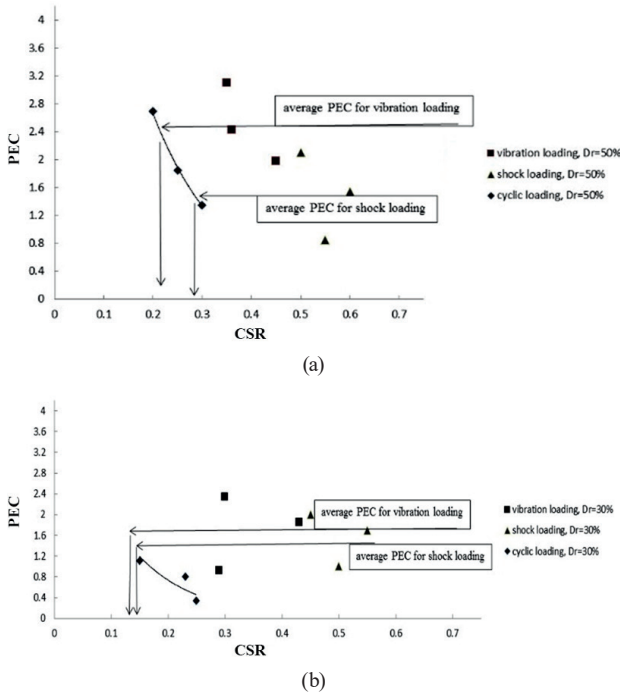


Fig. 11 Graphic illustration of how equivalent CSR is determined from experimental data; (a) $D_r = 50\%$, (b) $D_r = 30\%$

complicated time-domain characteristics of ground motions in both the stress method and the energy-based method.

Statistically, more experiments on different records are needed to evaluate the effect of these ground motion characteristics on the correction coefficients.

3.4 Analysis of the 1999 Chi-Chi Earthquake loading

To investigate soil behavior under shock and vibration loadings more precisely, the three main features of the Earth's motion (amplitude, frequency content, and duration of motion) were considered.

3.4.1 Amplitude parameters

Amplitude parameters include maximum acceleration, maximum velocity, and maximum displacement. The six records of the 1999 Chi-Chi Earthquake were considered at different stations. As previously stated, records obtained from stations 4 to 6 were categorized as shock type, and records from stations 1 to 3 were categorized as vibration type.

With shock loads No. 4, 5, and 6, the stations' horizontal distances from the epicenter were 19.04 km, 56.03 km, and 2.74 km, respectively. With vibration loads No.1, 2, and 3, they were 56.67 km, 57.5 km, and 56.93 km, respectively. So, the horizontal distance of station 5 was approximately equal to the horizontal distances of stations 1 to 3 is approximately equal. Therefore, this equality was a suitable criterion for the study of records.

According to Table 2, the maximum acceleration of the shock records at stations 4 to 6, was equal to 0.17, 0.12, and 0.42, respectively. This value for the vibrational records at stations 1 to 3, was 0.05, 0.04, and 0.06. Therefore, the shock records received higher maximum acceleration values. At the same distance from the earthquake epicenter (record 5), and the vibrational records of stations 1 to 3 (Table 2), the maximum acceleration value of the shock record was almost double the magnitude of the vibrational record.

According to previous studies, Earth's motion with a higher maximum acceleration is more destructive, so shock records are more destructive than vibration records.

3.4.2 Frequency content parameters

The content of the frequency describes how the range of motion of the Earth is distributed across different frequencies. The Fourier range spectra clearly depict the Earth's

Table 7 The Correction coefficients for different relative densities based on the energy method

No		PEC	$\left(\frac{q_{max,l}}{2\sigma'_c}\right)_{av}$	$\left(\frac{q_{u,l}}{2\sigma'_c}\right)_{20}$	$(C_{irr})_{av}$	N	
$D_r = 50\%$	1						
	2	Vibration type	2.5	0.39	0.21	0.54	65
	3						
	4						
	5	Shock type	1.5	0.55	0.28	0.51	15
	6						
$D_r = 30\%$	1						
	2	Vibration type	1.71	0.34	0.12	0.35	42
	3						
	4						
	5	Shock type	1.57	0.5	0.13	0.26	39
	6						

motion frequency content by showing both the amplitude distribution across different frequencies (or periods) and the strong motion of the Earth. Figs. 12 and 13 show the Fourier range spectra for the components of the 1999 Chi-Chi Earthquake movement at 6 different stations.

In the case of shock records, the maximum peak of the Fourier range occurred at a lower frequency (longer period), whereas in the vibrational records, the maximum value of the Fourier range was at higher frequencies (shorter period). At an equal distance from the epicenter of

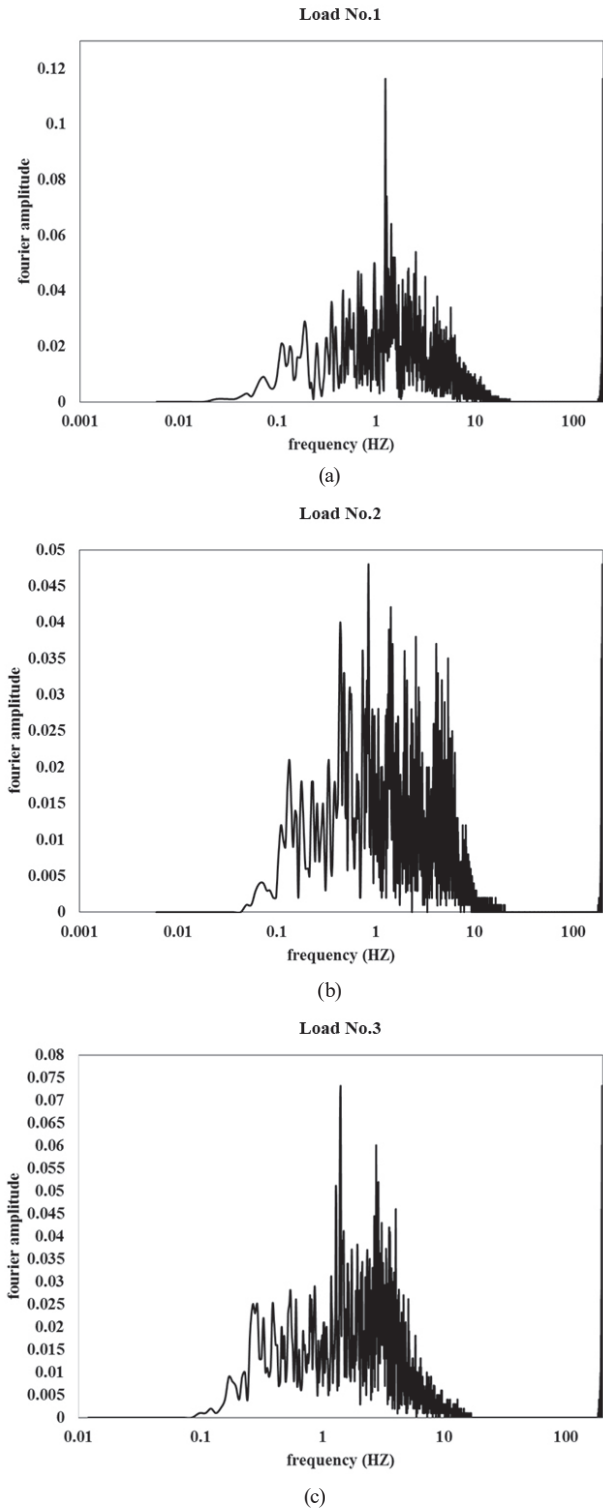


Fig. 12 The Fourier range spectra for the components of the 1999 Chi-Chi Earthquake movement for vibration loading (a) load No.1, (b) load No.2, (c) load No.3

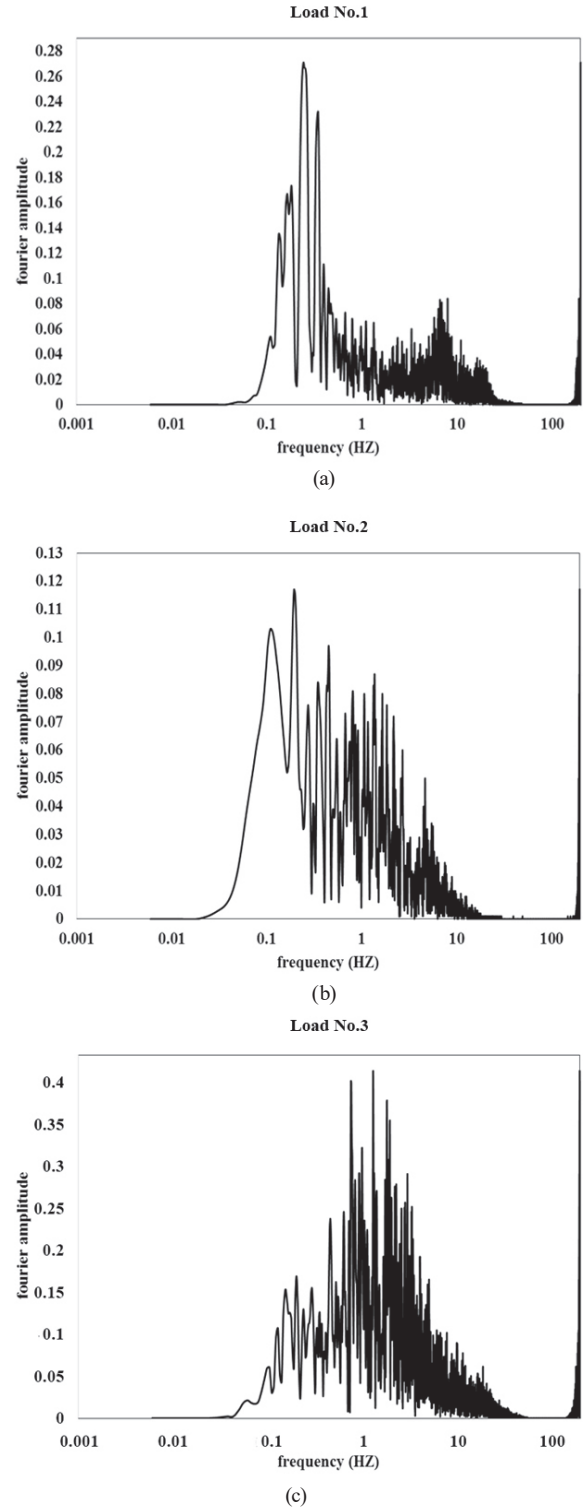


Fig. 13 The Fourier range spectra for the components of the 1999 Chi-Chi Earthquake movement for shock loading (a) load No.4, (b) load No.5, (c) load No.6

the earthquake in shock record No.5, the peak frequency of the Fourier amplitude occurred at a frequency of 0.201 Hz whereas this value for the vibrational records of No. 1 to 3 was equal to 1.245 Hz, 0.848 Hz, and 1.404 Hz, respectively. Therefore, for shock record, the Fourier amplitude peaked at a lower frequency than in the vibrational records, so larger energy was released at a lower frequency. Given the characteristics of the parameters of the frequency content of two types of shock and vibrational records, we conclude that shock records are stronger at a smaller frequency than vibration records. Therefore, they release more energy at a lower frequency and are more destructive.

Additionally, the values of (v_{\max}/a_{\max}) were calculated for all records at different stations during the 1999 Chi-Chi Earthquake. v_{\max} refers to the peak velocity of ground motion, which is the maximum speed at which the ground moves during an earthquake. It is usually expressed in units of cm/s or m/s. The shock records for load No. 4, 5, and 6 had (v_{\max}/a_{\max}) values of 0.224, 0.326, and 0.142 seconds respectively, while the vibration records for loads No. 1 to 3 had values of 0.122, 0.075, and 0.098 seconds, respectively. All the shock records had significantly higher (v_{\max}/a_{\max}) values than the vibration records, indicating that the shock-type loadings had more energy than the vibration-type records. This is because velocity represents the energy of the record, and the higher values for the shock records suggest that they had more energy than the vibration records.

Comparing the results obtained from the Fourier amplitude and the value of (v_{\max}/a_{\max}) , showed that the shock records had higher values in all frequencies compared to the vibrational records. Therefore, it can be concluded that the frequency content of the shock records was higher than that of the vibration records.

3.4.3 Effective earthquake duration

The duration of strong earth motion has a profound effect on earthquake-induced failures. Many physical processes, such as reducing the stiffness and increasing the water pressure of loose sand, are dependent on the number of cycles of loading that occur during an earthquake. The effective duration of an earthquake is the time period during which over 90% of the earthquake's energy is released [48]. This time period is scaled based on the 0.05–0.95 Arias intensity range. This parameter was calculated for all records.

At the same distance from the epicenter, the effective earthquake duration for shock record No. 5 was 24.7 seconds, while the corresponding values for vibration stations

1 to 3 were 39.07, 38, and 33.94 seconds, respectively. Furthermore, the effective earthquake durations for shock loadings 4 and 6 were 31.5 and 28 second, respectively. Thus, by increasing the effective earthquake duration of records, vibrational records have a greater potential to cause liquefaction than shock records [48].

3.4.4 Arias intensity

Moreover, Arias intensity values were calculated for all records. These values for shock-induced earthquakes of 4 to 6 were 0.593 m/sec, 0.236 m/sec, and 3.656 m/sec and for vibrating earthquakes of 1 to 3 were equal to 0.099 m/sec, 0.054 m/sec, and 0.08 m/sec, respectively.

Calculated values indicate that the amount of Arias intensity in shock loading was greater than the vibration type. Previous research indicates that the Arias intensity tends to rise as seismic recording stations are located closer to the earthquake epicenter. At a given distance from the epicenter of the earthquake, the Arias intensity of the shock record is higher than the vibration ones.

Consequently, shock records had more energy levels than vibration records, but the effective earthquake duration of vibration loads was longer than shock loads. In addition, the number of cycles in vibration records was much higher than that of shock loading. Therefore, shock loading had less potential to cause liquefaction than vibration loading.

According to the energy method and stress method, the result from the analysis of earthquake loading in the Chi-Chi area was consistent with the correction coefficient and the equivalent number of cycles that were calculated for shock and vibration loading. The correction coefficient of shock records was less than the vibration records at all considered values of the relative density of the soil.

4 Conclusions

Soil behavior under random earthquake loading depends on the specifications of the type of acceleration applied to the soil. In this study, earthquake acceleration was applied as deviator stress to the specimens, and the apparent forms of loading were investigated. The earthquake-induced loads were categorized into either shock or vibration types according to the number of cycles that reached 0.65 PGA. The stress method, which was derived from the assessment of soil liquefaction potential, was utilized to determine the stress correction coefficient for two different types of random earthquake loading. This coefficient was then adjusted for 20 cycles of uniform sinusoidal loading and the number of acceleration cycles that attained 0.65 PGA.

Major conclusions are summarized as follows:

- Compared to vibration loading, shock loading required a higher level of stress for liquefaction to occur than vibration loading.
- The results obtained from the stress method indicate that shock wave loading had the least potential to cause liquefaction. In contrast, the vibration type of loading had the greatest potential for liquefaction.
- An increase in pore-water pressure and subsequently, an increase in the stress correction coefficient were observed with an increase in the relative density of specimens from 30% to 50% in cyclic uniform loading.
- The form of irregular loading became more uniform as the correction coefficient approached a value of 1.0 in both methods (based on the number of cycles that reached 0.65 PGA and on the equivalent 20 cycles).
- The liquefaction potential of vibration records was higher compared to shock records, even at a similar (PGA). This was because vibration records had a higher number of acceleration cycles in their vibration waveform, compared to shock records that only reach 0.65PGA. Additionally, the effective duration of vibration records was also higher, contributing further to their higher liquefaction potential.
- The amount of dissipated energy in the specimens was slight at the beginning, but it increased suddenly after the occurrence of liquefaction.
- The amount of PEC in the sand was related to the loading range and form. This value was higher in vibration loading due to the application of more significant changes in the deviator stress compared to shock loading.
- The C_{irr} of the sand increased while the relative density of the specimens (30% and 50%) increased. It is noteworthy that the relative density played a significant role in governing the onset of liquefaction of cohesionless specimens subjected to seismic loading in both methods.
- By comparing the correction coefficients obtained from the two methods of stress and energy, for the two cases of earthquake random loading (shock and vibration), it can be concluded that the amount of the correction coefficient does not differ significantly but the main difference between the stress and energy methods is in the number of the equivalent cycles of the uniform sinusoidal stress. In the energy method, the number of equivalent cycles increases as the random loading form becomes more vibrational.

The analysis of records from the 1999 Chi-Chi Earthquake reveals that shock loading exhibits higher energy levels and frequency content than vibration loading. However, despite the shorter effective earthquake duration of shock loading, the number of cycles in the vibrational records is significantly greater. This results in a higher potential for liquefaction under vibration loading than shock loading, indicating that shock records at 30% and 50% densities should have a smaller correction coefficient than vibrational records obtained from both stress and energy methods. Therefore, it is not accurate to assume a single correction coefficient for all records due to the complex time-domain characteristics of ground motions.

References

- [1] Sladen, J. A., D'hollander, R. D., Krahn, J. "The liquefaction of sands, a collapse surface approach", *Canadian Geotechnical Journal*, 22(4), pp. 564–578, 1985.
<https://doi.org/10.1139/t85-076>
- [2] Demir, S. "Numerical Investigation of the Effects of Ground Motion Characteristics on the Seismic Behavior of Liquefiable Soil", *Periodica Polytechnica Civil Engineering*, 67(1), pp. 24–35, 2023.
<https://doi.org/10.3311/PPci.19683>
- [3] Bán, Z., Györi, E., Tóth, L., Gráczter, Z., Mahler, A. "Characterization and Liquefaction Hazard Assessment of Two Hungarian Liquefied Sites from the 1956 Dunaharaszti Earthquake", *Periodica Polytechnica Civil Engineering*, 64(3), pp. 713–721, 2020.
<https://doi.org/10.3311/PPci.15607>
- [4] Derakhshandi, M., Rathje, E. M., Hazirbaba, K., Mirhosseini, S. M. "The effect of plastic fines on the pore pressure generation characteristics of saturated sands", *Soil Dynamics and Earthquake Engineering*, 28(5), pp. 376–386, 2008.
<https://doi.org/10.1016/j.soildyn.2007.07.002>
- [5] Johari, A., Khodaparast, A. R., Javadi, A. A. "An Analytical Approach to Probabilistic Modeling of Liquefaction Based on Shear Wave Velocity", *Iranian Journal of Science and Technology*, *Transactions of Civil Engineering*, 43(1), pp. 263–275, 2019.
<https://doi.org/10.1007/s40996-018-0163-7>
- [6] Sağlam, S., Bakir, S. "Models for pore pressure response of low plastic fines subjected to repeated loads", *Journal of Earthquake Engineering*, 22(6), pp. 1027–1041, 2018.
<https://doi.org/10.1080/13632469.2016.1269697>

- [7] Nagy, L., Huszák, T. "Investigation of piping material", *Periodica Polytechnica Civil Engineering*, 56(2), pp. 233–238, 2012.
<https://doi.org/10.3311/pp.ci.2012-2.09>
- [8] Kwa, K. A., Airey, D. W. "Effects of fines on liquefaction behaviour in well-graded materials", *Canadian Geotechnical Journal*, 54(10), pp. 1460–1471, 2017.
<https://doi.org/10.1139/cgj-2017-0016>
- [9] Sim, W. W., Aghakouchak, A., Jardine, R. J. "Cyclic triaxial tests to aid offshore pile analysis and design", *Proceedings of the Institution of Civil Engineers-Geotechnical Engineering*, 166(2), pp. 111–121, 2013.
<https://doi.org/10.1680/geng.12.00056>
- [10] Seed, H. B. "Soil liquefaction and cyclic mobility evaluation for level ground during earthquake", *Journal of Geotechnical Engineering Division*, 105(2), pp. 211–254, 1979.
<https://doi.org/10.1061/AJGEB6.0000768>
- [11] Vucetic, M., Dobry, R. "Effect of Soil Plasticity on Cyclic Response", *Journal of Geotechnical Engineering*, 117(1), pp. 89–107 1991.
[https://doi.org/10.1061/\(ASCE\)0733-9410\(1991\)117:1\(89\)](https://doi.org/10.1061/(ASCE)0733-9410(1991)117:1(89))
- [12] Yang, Z. X., Li, X. S., Yang, J. "Undrained anisotropy and rotational shear in granular soil", *Géotechnique*, 57(4), pp. 371–384, 2007.
<https://doi.org/10.1680/geot.2007.57.4.371>
- [13] Seed, H. B., Idriss, I. M. "Simplified procedure for evaluating soil liquefaction potential", *Journal of the Soil Mechanics and Foundations Division*, 97(9), pp. 1249–1273, 1971.
<https://doi.org/10.1061/JSFEAQ.0001662>
- [14] Seed, H. B., Idriss, I. M., Makdisi, F., Banerjee, N. "Representation of irregular stress time histories by equivalent uniform stress series in liquefaction analyses", *Earthquake Engineering Research Center, University of California, Berkeley, CA, USA, Rep. EERC 75–29*, 1975.
- [15] Kwan, W. S., Sideras, S., El Mohtar, C. S., Kramer, S. "Pore Pressure Generation under Different Transient Loading Histories", presented at the 10th U.S. National Conference on Earthquake Engineering, *Frontiers of Earthquake Engineering*, Anchorage, Alaska, July, 21–25, 2014.
- [16] Ishihara, K., Yasuda, S. "Sand liquefaction due to irregular excitation", *Soils and Foundations*, 12(4), pp. 65–77, 1972.
https://doi.org/10.3208/sandf1972.12.4_65
- [17] Hui, S., Tang, L., Zhang, X., Wang, Y., Ling, X., Xu, B. "An investigation of the influence of near-fault ground motion parameters on the pile's response in liquefiable soil", *Earthquake Engineering and Engineering Vibration*, 17(4), pp. 729–745, 2018.
<https://doi.org/10.1007/s11803-018-0472-7>
- [18] Du, S., Chian, S. C. "Excess pore pressure generation in sand under non-uniform cyclic strain triaxial testing", *Soil Dynamics and Earthquake Engineering*, 109, pp. 119–131, 2018.
<https://doi.org/10.1016/j.soildyn.2018.03.016>
- [19] Pan, K., Yang, Z. X. "Evaluation of the liquefaction potential of sand under random loading conditions: Equivalent approach versus energy-based method", *Journal of Earthquake Engineering*, 24(1), pp. 59–83, 2020.
<https://doi.org/10.1080/13632469.2017.1398693>
- [20] Ishihara, K., Tatsuoka, F., Yasuda, S. "Undrained deformation and liquefaction of sand under cyclic stresses", *Soils and Foundations*, 15(1), pp. 29–44, 1975.
<https://doi.org/10.3208/sandf1972.15.29>
- [21] Ishihara, K., Yasuda, S. "Sand liquefaction under random earthquake loading condition", In: *Proceedings of the 5th World Conference on Earthquake Engineering*, Rome, Italy, 1973, pp. 329–338.
- [22] Sawada, S., Tsukamoto, Y., Ishihara, K. "Residual deformation characteristics of partially saturated sandy soils subjected to seismic excitation", *Soil Dynamics and Earthquake Engineering*, 26(2–4), pp. 175–182, 2006.
<https://doi.org/10.1016/j.soildyn.2004.11.024>
- [23] Tsukamoto, Y., Ishihara, K., Sawada, S. "Settlement of silty sand deposits following liquefaction during earthquakes", *Soils and Foundations*, 44(5), pp. 135–148, 2004.
https://doi.org/10.3208/sandf.44.5_135
- [24] Nemat-Nasser, S., Shokoh, A. "A unified approach to densification and liquefaction of cohesionless sand in cyclic shearing", *Canadian Geotechnical Journal*, 16(4), pp. 659–678, 1979.
<https://doi.org/10.1139/t79-076>
- [25] Chen, Y.-R., Chen, J.-W., Hsieh, S.-C., Chang, Y.-T. "Evaluation of soil liquefaction potential based on the nonlinear energy dissipation principles", *Journal of Earthquake Engineering*, 17(1), pp. 54–72, 2013.
<https://doi.org/10.1080/13632469.2012.691256>
- [26] Kokusho, T. "Liquefaction potential evaluations: energy-based method versus stress-based method", *Canadian Geotechnical Journal*, 50(10), pp. 1088–1099, 2013.
<https://doi.org/10.1139/cgj-2012-0456>
- [27] Law, K. T., Cao, Y. L., He, G. N. "An energy approach for assessing seismic liquefaction potential", *Canadian Geotechnical Journal*, 27(3), pp. 320–329, 1990.
<https://doi.org/10.1139/t90-043>
- [28] Okur, V., Ansal, A. "Evaluation of cyclic behavior of fine-grained soils using the energy method", *Journal of Earthquake Engineering*, 15(4), pp. 601–619, 2011.
<https://doi.org/10.1080/13632469.2010.507298>
- [29] Towhata, I., Ishihara, K. "Shear work and pore water pressure in undrained shear", *Soils and Foundations*, 25(3), pp. 73–84, 1985.
https://doi.org/10.3208/sandf1972.25.3_73
- [30] Javdanian, H., Heidari, A., Kamgar, R. "Energy-based estimation of soil liquefaction potential using GMDH algorithm", *Iranian Journal of Science and Technology, Transactions of Civil Engineering*, 41(3), pp. 283–295, 2017.
<https://doi.org/10.1007/s40996-017-0061-4>
- [31] Baziar, M. H., Jafarian, Y. "Assessment of liquefaction triggering using strain energy concept and ANN model: capacity energy", *Soil Dynamics and Earthquake Engineering*, 27(12), pp. 1056–1072, 2007.
<https://doi.org/10.1016/j.soildyn.2007.03.007>
- [32] Baziar, M. H., Sharafi, H. "Assessment of silty sand liquefaction potential using hollow torsional tests - An energy approach", *Soil Dynamics and Earthquake Engineering*, 31(7), pp. 857–865, 2011.
<https://doi.org/10.1016/j.soildyn.2010.12.014>
- [33] Jafariavval, Y., Derakhshani, A. "New formulae for capacity energy-based assessment of liquefaction triggering", *Marine Georesources & Geotechnology*, 38(2), pp. 214–222, 2020.
<https://doi.org/10.1080/1064119X.2019.1566297>

- [34] Jafarian, Y., Towhata, I., Baziar, M. H., Noorzad, A., Bahmanpour, A. "Strain energy based evaluation of liquefaction and residual pore water pressure in sands using cyclic torsional shear experiments", *Soil Dynamics and Earthquake Engineering*, 35, pp. 13–28, 2012. <https://doi.org/10.1016/j.soildyn.2011.11.006>
- [35] Pan, K., Yang, Z. "Undrained behavior of sand under cyclic paths that match storm-wave loading conditions", *Marine Georesources & Geotechnology*, 36(1), pp. 72–82, 2018. <https://doi.org/10.1080/1064119X.2017.1279697>
- [36] Tsuchida, H., Hayashi, S. "Estimation of liquefaction potential of sandy soils", In: *Proceedings of the Third Joint Meeting, US-Japan Panel on Wind and Seismic Effects, UJNR, Tokyo, Japan, 1971*, pp. 91–109.
- [37] Park, J. Y. "A critical assessment of moist tamping and its effect on the initial and evolving structure of dilatant triaxial specimens", PhD Thesis, Georgia Institute of Technology, 1999. <http://hdl.handle.net/1853/23949>
- [38] Yang, Z., Lit, X., Yang, J. "Quantifying and modelling fabric anisotropy of granular soils", *Geotechnique*, 85(4), pp. 237–248, 2008. <https://doi.org/10.1680/geot.2008.58.4.237>
- [39] Sze, H. Y., Yang, J. "Failure modes of sand in undrained cyclic loading: impact of sample preparation", *Journal of Geotechnical and Geoenvironmental Engineering*, 140(1), pp. 152–169, 2014. [https://doi.org/10.1061/\(ASCE\)GT.1943-5606.0000971](https://doi.org/10.1061/(ASCE)GT.1943-5606.0000971)
- [40] Derakhshandi, M., Rathje, E. M., Hazirbaba, K., Mirhosseini, S. M. "The effect of plastic fines on the pore pressure generation characteristics of saturated sands", *Soil Dynamics and Earthquake Engineering*, 28(5), pp. 376–386, 2008. <https://doi.org/10.1016/j.soildyn.2007.07.002>
- [41] Galandazadeh, A., Ahmadi, A. "Effects of anisotropic consolidation and stress reversal on the liquefaction resistance of sands and silty sands", *Geotechnical Engineering*, 43(2), pp. 33–39, 2012. https://doi.org/10.1007/978-3-540-79846-0_37
- [42] Youd, T. L., Idriss, I. M., Andrus, R. D., Arango, I., Castro, G., ..., Stokoe, K. H. "Liquefaction resistance of soils: summary report from the 1996 NCEER and 1998 NCEER/NSF workshops on evaluation of liquefaction resistance of soils", *Journal of Geotechnical and Geoenvironmental Engineering*, 127(10), pp. 297–313, 2001. [https://doi.org/10.1061/\(asce\)1090-0241\(2001\)127:10\(817\)](https://doi.org/10.1061/(asce)1090-0241(2001)127:10(817))
- [43] Liu, C., Xu, J. "Experimental study on the effects of initial conditions on liquefaction of saturated and unsaturated sand", *International Journal of Geomechanics*, 15(6), 04014100, 2015. [https://doi.org/10.1061/\(ASCE\)GM.1943-5622.0000350](https://doi.org/10.1061/(ASCE)GM.1943-5622.0000350)
- [44] Peacock, W. H., Seed, H. B. "Sand liquefaction under cyclic loading simple shear conditions", *Journal of Soil Mechanics and Foundations Division*, 94(3), pp. 689–708, 1968. <https://doi.org/10.1061/JSFEAQ.0001135>
- [45] Tatsuoka, F., Muramatsu, M., Sasaki, T. "Cyclic undrained stress-strain behavior of dense sands by torsional simple shear test", *Soils and Foundations*, 22(2), pp. 55–70, 1982. https://doi.org/10.3208/sandf1972.22.2_55
- [46] Katebi, B., Derakhshandi, M., Ghalandarzadeh, A., Ganjian, N. "Experimental investigation of the effect of relative densities and type of loading on sand liquefaction under irregular earthquake loading", *Amirkabir Journal of Civil Engineering*, 54(1), pp. 3–6, 2022. <https://doi.org/10.22060/ceej.2019.16278.6175>
- [47] Green, R. A., Mitchell, J. K., Polito, C. P. "An energy-based excess pore pressure generation model for cohesionless soils", presented at the John Booker Memorial Symposium, Sidney, Australia, Nov. 16–17, 2000.
- [48] Unjoh, S., Kaneko, M., Kataoka, S., Nagaya, K., Matsuoka, K. "Effect of earthquake ground motions on soil liquefaction", *Soils and Foundations*, 52(5), pp. 830–841, 2012. <https://doi.org/10.1016/j.sandf.2012.11.006>